First Results from KamLAND: Evidence for Reactor Antineutrino Disappearance

K. Eguchi,[1] S. Enomoto,[1] K. Furuno,[1] J. Goldman,[1] H. Hanada,[1] H. Ikeda,[1] K. Ikeda,[1] K. Inoue,[1] K. Ishihara,[1] W. Itoh,[1] T. Iwamoto,[1] T. Kawaguchi,[1] T. Kawashima,[1] H. Kinoshita,[1] Y. Kishimoto,[1] M. Koga,[1] Y. Koseki,[1] T. Maeda,[1] T. Mitsui,[1] M. Motoki,[1] K. Nakajima,[1] M. Nakajima,[1] T. Nakajima,[1] H. Ogawa,[1] K. Owada,[1] T. Sakabe,[1] I. Shimizu,[1] J. Shirai,[1] F. Suekane,[1] A. Suzuki,[1] K. Tada,[1] O. Tajima,[1] T. Takayama,[1] K. Tamae,[1] H. Watanabe,[1] J. Busenitz,[2] Z. Djurcic,[2] K. McKinny,[2] D.-M. Mei,[2] A. Piepke,[2] E. Yakushev,[2] B. E. Berger,[3] Y. D. Chan,[3] M. P. Decowski,[3] D. A. Dwyer,[3] S. J. Freedman,[3] Y. Fu,[3] B. K. Fujikawa,[3] K. M. Heeger,[3] K. T. Lesko,[3] K.-B. Luk,[3] H. Murayama,[3] D. R. Nygren,[3] C. E. Okada,[3] A. W. P. Poon,[3] H. M. Steiner,[3] L. A. Winslow,[3] G. A. Horton-Smith,[4] R. D. McKeown,[4] J. Ritter,[4] B. Tipton,[4] P. Vogel,[4] C. E. Lane,[5] T. Miletic,[5] P. W. Gorham,[6] G. Guillian,[6] J. G. Learned,[6] J. Maricic,[6] S. Matsuno,[6] S. Pakvasa,[6] S. Dazeley,[7] S. Hatakeyama,[7] M. Murakami,[7] R. C. Svoboda,[7] B. D. Dieterle,[8] M. DiMauro,[8] J. Detwiler,[9] G. Gratta,[9] K. Ishii,[9] N. Tolich,[9] Y. Uchida,[9] M. Batygov,[10] W. Bugg,[10] H. Cohn,[10] Y. Efremenko,[10] Y. Kamyshkov,[10] A. Kozlov,[10] Y. Nakamura,[10] L. De Braeckeleer,[11] C. R. Gould,[11] H. J. Karwowski,[11] D. M. Markoff,[11] J. A. Messimore,[11] K. Nakamura,[11] R. M. Rohm,[11] W. Tornow,[11] A. R. Young,[11] and Y.-F. Wang[12]

(KamLAND Collaboration)

[1]*Research Center for Neutrino Science, Tohoku University, Sendai 980-8578, Japan*
[2]*Department of Physics and Astronomy, University of Alabama, Tuscaloosa, Alabama 35487*
[3]*Physics Department, University of California at Berkeley and Lawrence Berkeley National Laboratory, Berkeley, California 94720*
[4]*W. K. Kellogg Radiation Laboratory, California Institute of Technology, Pasadena, California 91125*
[5]*Physics Department, Drexel University, Philadelphia, Pennsylvania 19104*
[6]*Department of Physics and Astronomy, University of Hawaii at Manoa, Honolulu, Hawaii 96822*
[7]*Department of Physics and Astronomy, Louisiana State University, Baton Rouge, Louisiana 70803*
[8]*Physics Department, University of New Mexico, Albuquerque, New Mexico 87131*
[9]*Physics Department, Stanford University, Stanford, California 94305*
[10]*Department of Physics and Astronomy, University of Tennessee, Knoxville, Tennessee 37996*
[11]*Triangle Universities Nuclear Laboratory, Durham, North Carolina 27708*
and Physics Departments at Duke University, North Carolina State University,
and the University of North Carolina at Chapel Hill
[12]*Institute of High Energy Physics, Beijing 100039, People's Republic of China*
(Received 6 December 2002; published 17 January 2003)

KamLAND has measured the flux of $\bar{\nu}_e$'s from distant nuclear reactors. We find fewer $\bar{\nu}_e$ events than expected from standard assumptions about $\bar{\nu}_e$ propagation at the 99.95% C.L. In a 162 ton · yr exposure the ratio of the observed inverse β-decay events to the expected number without $\bar{\nu}_e$ disappearance is $0.611 \pm 0.085(\text{stat}) \pm 0.041(\text{syst})$ for $\bar{\nu}_e$ energies > 3.4 MeV. In the context of two-flavor neutrino oscillations with CPT invariance, all solutions to the solar neutrino problem except for the "large mixing angle" region are excluded.

DOI: 10.1103/PhysRevLett.90.021802 PACS numbers: 14.60.Pq, 26.65.+t, 28.50.Hw, 91.65.Dt

The primary goal of the Kamioka Liquid Scintillator Anti-Neutrino Detector (KamLAND) [1] is a search for the oscillation of $\bar{\nu}_e$'s emitted from distant power reactors. The long baseline, typically 180 km, enables KamLAND to address the oscillation solution [2,3] of the "solar neutrino problem" [4] with $\bar{\nu}_e$'s under laboratory conditions. The inverse β-decay reaction, $\bar{\nu}_e + p \rightarrow e^+ + n$ is used to detect $\bar{\nu}_e$'s in liquid scintillator (LS) [5]. Detecting both the e^+ and the delayed 2.2 MeV γ-ray from neutron capture on a proton is a powerful tool for reducing background. This Letter presents first results from an analysis of 162 ton · yr (145.1 d) of the reactor $\bar{\nu}_e$ data.

KamLAND occupies the site of the earlier Kamiokande [6], under 2700 m.w.e. of rock resulting in 0.34 Hz of cosmic-ray muons in the detector. Shown in Fig. 1, the neutrino detector/target is 1 kton of ultrapure LS contained in a 13-m-diameter spherical balloon made of 135-μm-thick transparent nylon/EVOH (ethylene vinyl alcohol copolymer) composite film. A network of Kevlar ropes supports and constrains the balloon. The LS is 80% dodecane, 20% pseudocumene (1,2,4-trimethylbenzene), and 1.52 g/liter of PPO (2,5-diphenyloxazole) as a fluor. A buffer of dodecane and isoparaffin oils between the balloon and an 18-m-diameter spherical stainless-steel containment vessel shields the LS from external radiation.

 © 2003 The American Physical Society

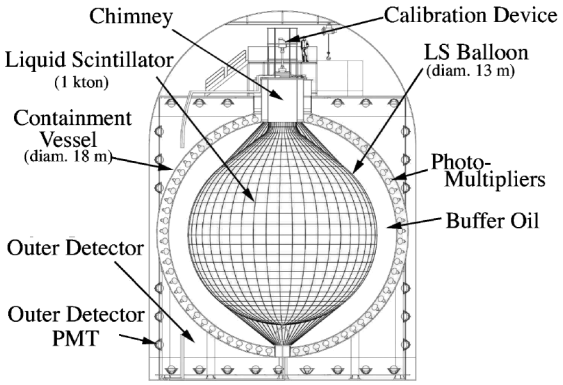

FIG. 1. Schematic diagram of the KamLAND detector.

During filling water extraction and nitrogen stripping [7] purified the LS and buffer oil (BO). The buffer oil density is 0.04% lower than the LS. A 1879 photomultiplier tube array, mounted on the containment vessel, completes the inner detector (ID). There are 1325 newly developed fast 17-inch-diameter photomultiplier tubes (PMTs) and 554 older Kamiokande 20-inch PMTs [8]. The total photocathode coverage is 34% but only the 17-inch PMTs with 22% coverage are used for the present analysis. A 3-mm-thick acrylic barrier at 16.6-m diameter reduces radon from PMT glass in the LS. The containment vessel is surrounded by a 3.2 kton water-Cherenkov detector with 225 20-inch PMTs. This outer detector (OD) absorbs γ rays and neutrons from surrounding rock and acts as a tag for cosmic-ray muons. The primary ID trigger threshold is 200 PMT hits, corresponding to about 0.7 MeV. The threshold goes to 120 hits for 1 msec after a primary trigger. The OD trigger threshold corresponds to $> 99\%$ tagging efficiency.

Energy response in the 0.5 to 7.5 MeV range is calibrated with ^{68}Ge, ^{65}Zn, ^{60}Co, and Am-Be γ-ray sources deployed at various positions along the vertical axis. Detected energy is obtained from the number of observed photoelectrons (p.e.) after corrections for gain variation, solid angle, density of PMTs, shadowing by suspension ropes, and transparencies of the LS and BO. Figure 2(a) shows the fractional deviation of the reconstructed energies from the known source energies. The ^{68}Ge and ^{60}Co sources emit two coincident γ rays and are plotted at an average energy in Fig. 2(a). The observed energy resolution is $\sim 7.5\%/\sqrt{E(\mathrm{MeV})}$.

The energy scale is augmented from studies of the radiation from ^{40}K and ^{208}Tl and Bi-Po contaminants, as well as ^{12}B- and ^{12}N-spallation products, and γ rays from neutron capture on protons and ^{12}C. The reconstructed energy varies by less than 0.5% within a 10-m-diameter volume except for 1.6% variations near the chimney. The energy scale is stable to 0.6% during the run. Corrections for quenching and Cherenkov light production are included, and contribute to the systematic error in Fig. 2(a). The estimated systematic error in the energy is 1.9% at our 2.6 MeV analysis threshold giving a 2.1% uncertainty in the rate above threshold.

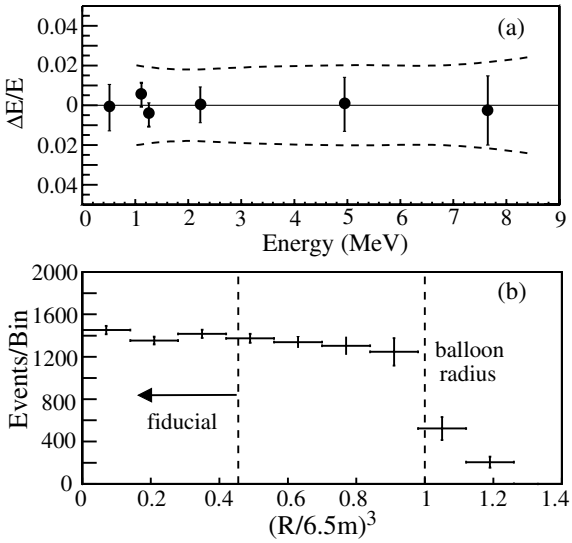

FIG. 2. (a) The fractional difference of the reconstructed average energies and known source γ energies. The dashed lines show the adopted systematic error. (b) The R^3 vertex distribution of 2.2 MeV neutron capture γ's. The level of uniformity over the fiducial volume is used in the estimate of the fiducial volume uncertainty.

Event locations are reconstructed from the timing of PMT hits. After energy-dependent radial adjustments, the known source positions are reconstructed to ~ 5 cm; the typical position resolution is ~ 25 cm. Vertex reconstruction performance throughout the LS volume is verified by reproducing the uniform distribution of 2.2 MeV capture γ's from spallation neutrons, as shown in Fig. 2(b).

The data presented in this Letter were collected from March 4 through October 6, 2002. We obtained 370×10^6 events in 145.1 d of live time at an average trigger rate of $\simeq 30$ Hz. Events with less than 10 000 p.e. ($\sim$30 MeV) and no prompt OD tag are "reactor-$\bar{\nu}_e$ candidates"; more energetic events are "muon candidates."

The selection cuts for $\bar{\nu}_e$ events are the following: (i) fiducial volume ($R < 5$ m), (ii) time correlation ($0.5\ \mu\mathrm{sec} < \Delta T < 660\ \mu\mathrm{sec}$), (iii) vertex correlation ($\Delta R < 1.6$ m), (iv) delayed energy ($1.8\ \mathrm{MeV} < E_{\mathrm{delay}} < 2.6\ \mathrm{MeV}$), and (v) a requirement that the delayed vertex position be more than 1.2 m from the central vertical axis to eliminate background from LS monitoring thermometers. The overall efficiency for the events from criteria (ii)–(v) including the effect of (i) on the delayed vertex is $(78.3 \pm 1.6)\%$.

Including annihilation, the detected energy for positrons is the kinetic energy plus twice the rest energy; thus on the average e^+ from $\bar{\nu}_e$ events yield $E_{\mathrm{prompt}} = E_{\bar{\nu}_e} - \bar{E}_n - 0.8$ MeV, where $\bar{E}_n$ is the average recoil energy of the neutron. Antineutrinos from ^{238}U and ^{232}Th in the Earth, "geoneutrinos" ($\bar{\nu}_{\mathrm{geo}}$) can produce

events with $E_{\text{prompt}} < 2.49$ MeV. Model Ia in Ref. [9] predicts about 9 $\bar{\nu}_{\text{geo}}$ events in our data set. However, the abundances and distributions of U and Th are not well known. We employ (vi) a prompt energy cut, $E_{\text{prompt}} > 2.6$ MeV, to avoid ambiguity in the present analysis.

The fiducial volume is estimated using the expected uniform distribution of spallation-product neutron-capture events shown in Fig. 2(b). The ratio of events in the fiducial volume to the total volume agrees with the geometric fiducial fraction to within 4.1%. This method is also used for higher energy events from ^{12}N, ^{12}B β's following muon spallation; the agreement is within 3.5%. Accounting for the 2.1% uncertainty in the total LS mass, we estimate a 4.6% uncertainty in the fiducial volume. The LS density is 0.780 g/cm^3 at 11.5 °C; the expected hydrogen-to-carbon ratio of 1.97 was verified by elemental analysis to $\pm 2\%$. The specific gravity is measured to 0.01% precision and we assign an additional 0.1% error from the uncertainty in the temperature. The 408 ton fiducial mass thus contains 3.46×10^{31} free target protons.

The trigger efficiency was determined to be 99.98% with LED light sources. The combined efficiency of the electronics, data acquisition, and event reconstruction was studied using time distributions of uncorrelated events from calibration γ sources. We find that this combined efficiency is better than 99.98%. The vertex fitter yields $> 99.9\%$ efficiency within 2 m of known source positions. With calibrated ^{60}Co and ^{65}Zn sources, the overall efficiency was checked to the 3% source-strength uncertainties. The detection efficiency for delayed events from the Am-Be source (4.4 MeV prompt γ and 2.2 MeV delayed neutron capture γ within 1.6 m) was verified to 1% certainty.

Studies of Bi-Po sequential decays indicate that the effective equilibrium concentrations of ^{238}U and ^{232}Th in the LS are $(3.5 \pm 0.5) \times 10^{-18}$ g/g and $(5.2 \pm 0.8) \times 10^{-17}$ g/g, respectively. The observed background energy spectrum indicates that ^{40}K contamination is less than 2.7×10^{-16} g/g. The extremely low level of U and Th contamination in the LS provides an optimistic prospect for future solar neutrino experiments with KamLAND. The flat accidental background, observed in a delayed time window of 0.020–20 sec, is 0.0086 ± 0.0005 events for the present data set.

The most serious source of external γ rays from ^{208}Tl ($E_\gamma \leq 3$ MeV) is strongly suppressed by the fiducial volume cut (i). At higher energies, the background is dominated by spallation products from energetic muons. We observe ~3 000 neutron events/day/kton. We also expect ~1 300 events/day/kton [10] for various unstable products.

Single neutrons are easily suppressed with a 2-msec veto following a muon. Care is required to avoid neutrons which mimic the $\bar{\nu}_e$ delayed coincidence signal. Most external fast neutrons are produced by muons which pass through both the OD and the surrounding rock. This background is studied by detecting delayed coincidence events tagged with a muon detected by only the OD. As expected, events concentrate near the balloon edge. The background in the fiducial volume is estimated by extrapolating the distribution of vertex positions and accounting for the 92% OD reconstruction efficiency. The number of background events due to neutrons from the surrounding rock is estimated from the OD-tagged data scaled by the relative neutron production and the shielding factor of the relevant materials. The estimated total fast neutron background is less than 0.5 events in the entire data set.

Most radioactive spallation products simply beta decay, and are effectively suppressed by requiring a delayed neutron. Delayed neutron emitters such as ^{8}He ($T_{1/2} = 119$ msec) and ^{9}Li (178 msec) are eliminated by two time/geometry cuts: (a) a 2-sec veto in the entire fiducial volume following a "showering muon" (more than 10^6 p.e., ~3 GeV, extra energy deposition), (b) for other muons, delayed events within 2 sec and 3 m of the muon track are rejected. The cut efficiency is estimated from the observed correlation of spallation neutrons with muon tracks. The remaining ^{8}He and ^{9}Li background is estimated to be 0.94 ± 0.85. The dead time from spallation cuts is 11.4%. This is checked by constructing the time distribution of the events following a detected muon to separate the short-lived spallation-produced activities from $\bar{\nu}_e$ candidates. The uncorrelated $\bar{\nu}_e$ distribution has a time constant of $1/R_\mu \simeq 3$ sec, where R_μ is the muon rate. Spallation products all have a shorter time constant (~ 0.2 sec). The two selected methods agree to 3% accuracy. As shown in Table I, the total number of expected background events is 1 ± 1, where the fast neutron contribution is included in the error estimate.

Instantaneous thermal power, burnup, and fuel exchange records for all commercial Japanese power reactors are provided by the power companies. The thermal power generation is checked with the independent records of electric power generation. The fission rate for each fissile isotope is calculated as a function of time and the systematic uncertainty in the $\bar{\nu}_e$ flux is 1%. Averaged over live time, the relative fission yields from fuel components are ^{235}U: ^{238}U: ^{239}Pu: ^{241}Pu = 0.568 : 0.078 : 0.297 : 0.057. The $\bar{\nu}_e$ spectrum per fission with a 2.5% error

TABLE I. Background summary.

Background	Number of events
Accidental	0.0086 ± 0.0005
^{9}Li/^{8}He	0.94 ± 0.85
Fast neutron	<0.5
Total B.G. events	1 ± 1

TABLE II. Estimated systematic uncertainties (%).

Total LS mass	2.1	Reactor power	2.0
Fiducial mass ratio	4.1	Fuel composition	1.0
Energy threshold	2.1	Time lag	0.28
Efficiency of cuts	2.1	$\bar{\nu}$ spectra [11]	2.5
Live time	0.07	Cross section [14]	0.2
Total systematic error			6.4%

are taken from [11]. This neutrino spectrum has been tested to a few percent with short-baseline reactor $\bar{\nu}_e$ experiments [5,12]. The finite lifetimes of fission products introduce a 0.28% uncertainty to the $\bar{\nu}_e$ flux. The contribution from Korean reactors is estimated to be $(2.46 \pm 0.25)\%$ based on reported electric power generation. The rest of the World's reactors contribute $(0.70 \pm 0.35)\%$ from an estimate using reactor specifications from the International Nuclear Safety Center [13]. In the absence of $\bar{\nu}_e$ disappearance the expected number of $\bar{\nu}_e$ events is 86.8 ± 5.6; the systematic error contributions are listed in Table II.

The antineutrinos at KamLAND are provided by many nuclear reactors but the flux is actually dominated by a few powerful reactors at an average distance of ~180 km. More than 79% of the flux is from 26 reactors between 138–214 km away. One close reactor at 88 km contributes 6.7%; other reactors are more than 295 km away. The relatively narrow band of distances allows KamLAND to be sensitive to spectral distortions for certain oscillation parameters.

Figure 3 shows the energy distribution of delayed coincidence events with no energy cuts. A well-separated cluster of 2.2 MeV capture γ's is evident. One observed event with delayed energy around 5 MeV and prompt energy of about 3.1 MeV (not shown in Fig. 3) is consistent with the expected neutron radiative capture rate on ^{12}C.

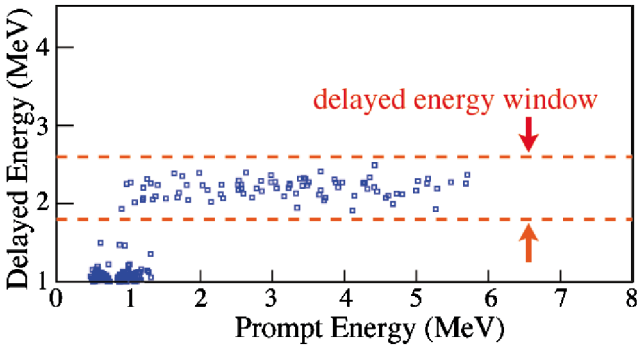

FIG. 3 (color). Distribution of $\bar{\nu}_e$ candidates after fiducial volume, time, vertex correlation, and spallation cuts are applied. For $\bar{\nu}_e$ events the prompt energy is attributed to positrons and the delayed energy to neutron capture. Events within the horizontal lines bracketing the delayed energy of 2.2 MeV are consistent with thermal neutron capture on protons.

The observed space-time correlation of the prompt and delayed events agrees with expectations, and the measured capture time of 188 ± 23 μsec is consistent with predictions for LS. After applying all the prompt and delayed energy cuts, 54 events remain. Accounting for ~1 background event the probability of a fluctuation from 86.8 expected is <0.05% by Poisson statistics. The ratio of observed reactor $\bar{\nu}_e$ events to expected in the absence of neutrino disappearance is

$$\frac{N_{\text{obs}} - N_{\text{BG}}}{N_{\text{expected}}} = 0.611 \pm 0.085(\text{stat}) \pm 0.041(\text{syst}).$$

Figure 4 shows the ratio of measured to expected flux for KamLAND as well as previous reactor experiments as a function of the average distance from the source.

The expected prompt positron spectrum with no oscillations and the best fit with reduced $\chi^2 = 0.31$ for 8 degrees of freedom for two-flavor neutrino oscillations above the 2.6 MeV threshold are shown in Fig. 5. A clear deficit of events is evident. At the 93% C.L. the data are consistent with a distorted spectrum shape expected from neutrino oscillations, but a scaled no-oscillation shape is also consistent at 53% C.L. as determined by Monte Carlo.

The neutrino oscillation parameter region for two-neutrino mixing is shown in Fig. 6. The dark shaded area is the MSW-LMA [19] region at 95% C.L. derived from [16]. The shaded region outside the solid line is excluded at 95% C.L. from the rate analysis with $\chi^2 \geq 3.84$ and

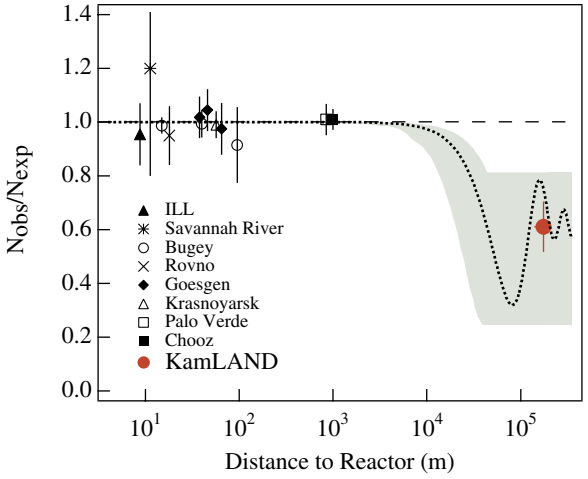

FIG. 4 (color). The ratio of measured to expected $\bar{\nu}_e$ flux from reactor experiments [15]. The solid circle is the KamLAND result plotted at a flux-weighted average distance of ~180 km. The shaded region indicates the range of flux predictions corresponding to the 95% C.L. LMA region from a global analysis of the solar neutrino data [16]. The dotted curve, $\sin^2 2\theta = 0.833$ and $\Delta m^2 = 5.5 \times 10^{-5}$ eV^2 [16], is representative of a best-fit LMA prediction and the dashed curve is expected for no oscillations.

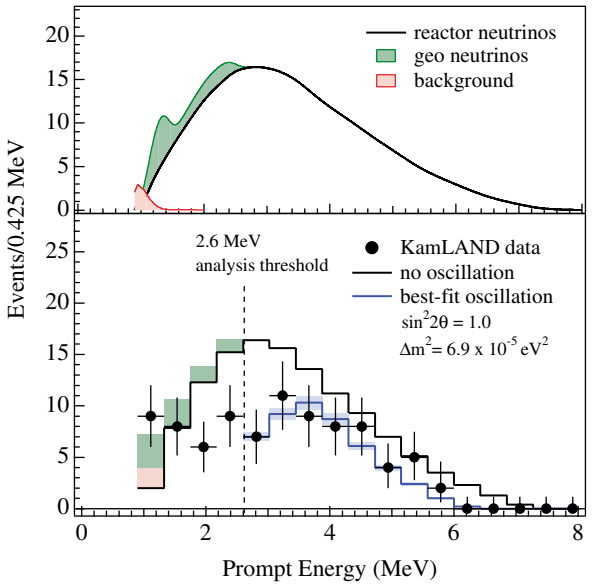

FIG. 5 (color). Upper panel: Expected reactor $\bar{\nu}_e$ energy spectrum along with $\bar{\nu}_{\text{geo}}$ (model Ia of [9]) and background. Lower panel: Energy spectrum of the observed prompt events (solid circles with error bars), along with the expected no oscillation spectrum (upper histogram, with $\bar{\nu}_{\text{geo}}$ and background shown) and best fit (lower histogram) including neutrino oscillations. The shaded band indicates the systematic error in the best-fit spectrum. The vertical dashed line corresponds to the analysis threshold at 2.6 MeV.

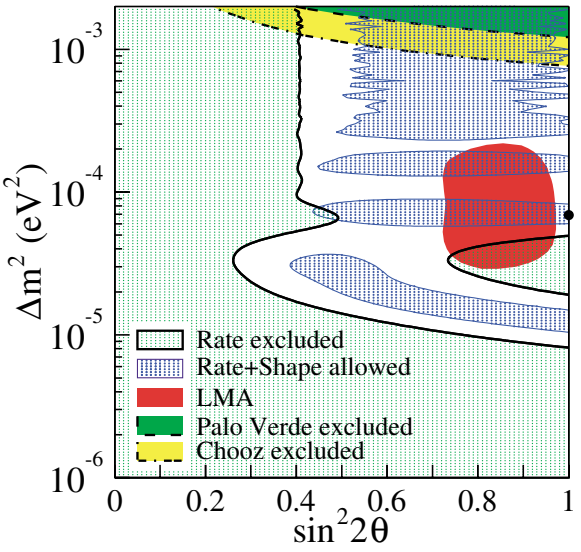

FIG. 6 (color). Excluded regions of neutrino oscillation parameters for the rate analysis and allowed regions for the combined rate and shape analysis from KamLAND at 95% C.L. At the top are the 95% C.L. excluded region from CHOOZ [17] and Palo Verde [18] experiments, respectively. The 95% C.L. allowed region of the large mixing angle (LMA) solution of solar neutrino experiments [16] is also shown. The solid circle shows the best fit to the KamLAND data in the physical region: $\sin^2 2\theta = 1.0$ and $\Delta m^2 = 6.9 \times 10^{-5}$ eV^2. All regions look identical under $\theta \leftrightarrow (\pi/2 - \theta)$ except for the LMA region from solar neutrino experiments.

$$\chi^2 = \frac{[0.611 - R(\sin^2 2\theta, \Delta m^2)]^2}{0.085^2 + 0.041^2}.$$

Here, $R(\sin^2 2\theta, \Delta m^2)$ is the expected ratio with the oscillation parameters.

The final event sample is evaluated using a maximum likelihood method to obtain the optimum set of oscillation parameters with the following χ^2 definition:

$$\begin{aligned}\chi^2 =& \chi^2_{\text{rate}}(\sin^2 2\theta, \Delta m^2, N_{\text{BG1}\sim 2}, \alpha_{1\sim 4}) \\ & - 2\log L_{\text{shape}}(\sin^2 2\theta, \Delta m^2, N_{\text{BG1}\sim 2}, \alpha_{1\sim 4}) \\ & + \chi^2_{\text{BG}}(N_{\text{BG1}\sim 2}) + \chi^2_{\text{distortion}}(\alpha_{1\sim 4}).\end{aligned}$$

L_{shape} is the likelihood function for the spectrum including experimental distortions. $N_{\text{BG1}\sim 2}$ are the estimated ^{9}Li and ^{8}He backgrounds and $\alpha_{1\sim 4}$ are parameters to account for the spectral effects of energy scale uncertainty, finite resolution, $\bar{\nu}_e$ spectrum uncertainty, and fiducial volume systematic error, respectively. Parameters are varied to minimize the χ^2 at each pair of $[\Delta m^2, \sin^2\theta]$ with a bound from $\chi^2_{\text{BG}}(N_{\text{BG1}\sim 2})$ and $\chi^2_{\text{distortion}}(\alpha_{1\sim 4})$. The best fit to the data in the physical region yields $\sin^2 2\theta = 1.0$ and $\Delta m^2 = 6.9 \times 10^{-5}$ eV^2 while the global minimum occurs slightly outside of the physical region at $\sin^2 2\theta = 1.01$ with the same Δm^2. These numbers can be compared to the best fit LMA values of $\sin^2 2\theta = 0.83$ and $\Delta m^2 = 5.5 \times 10^{-5}$ eV^2 from [16]. The 95% C.L. allowed regions from the spectrum shape analysis for $\Delta\chi^2 = 5.99$ and two parameters are shown in Fig. 6. The allowed regions displayed for KamLAND correspond to $0 < \theta < \frac{\pi}{4}$ consistent with the solar LMA solution, while the allowed regions in $\frac{\pi}{4} < \theta < \frac{\pi}{2}$ are the same [20] but do not include the solar solution.

The results from a spectral shape analysis with a 0.9 MeV threshold are consistent with the above result. In this low-energy analysis, the measured $\bar{\nu}_{\text{geo}}$ fluxes are free parameters. The numbers of $\bar{\nu}_{\text{geo}}$ events for the best fit are four for ^{238}U and five for ^{232}Th, which corresponds to $\sim$40 TW radiogenic heat generation according to model Ia in [9]. However, for the same model, $\bar{\nu}_{\text{geo}}$ production powers from 0 to 110 TW are still allowed at 95% C.L. with the same oscillation parameters.

If three neutrino generations are considered, the $\bar{\nu}_e$ survival probability depends on two mixing angles θ_{12} and θ_{13}. In the region close to the best fit KamLAND solution the survival probability is, to a very good approximation, given by

$$P(\bar{\nu}_e \to \bar{\nu}_e) \cong \cos^4\theta_{13}\left[1 - \sin^2 2\theta_{12}\sin^2\frac{\Delta m^2_{12} L}{4E_\nu}\right],$$

with $\Delta m^2_{12} \cong \Delta m^2$ from the two-flavor analysis above.

The CHOOZ experiment [17] established an upper limit of $\sin^2 2\theta_{13} < 0.15$, or $\cos^4\theta_{13} \geq 0.92$. Our best fit result corresponds approximately to $0.86 < \sin^2 2\theta_{12} < 1.0$.

In summary, KamLAND demonstrated reactor $\bar{\nu}_e$ disappearance at long baselines and high confidence level (99.95%) for the first time. One expects a negligible reduction of $\bar{\nu}_e$ flux from the SMA, LOW, and VAC solar neutrino solutions, and the LMA region is the only remaining oscillation solution consistent with the KamLAND result assuming CPT invariance. The allowed LMA region is constrained by KamLAND. Future KamLAND measurements with improved statistical precision and reduced systematic errors will provide precision determinations of neutrino oscillation parameters.

The KamLAND experiment is supported by the Center of Excellence program of the Japanese Ministry of Education, Culture, Sports, Science and Technology, and funding from the United States Department of Energy. The reactor data are provided courtesy of the following electric associations in Japan; Hokkaido, Tohoku, Tokyo, Hokuriku, Chubu, Kansai, Chugoku, Shikoku and Kyushu Electric Power Companies, Japan Atomic Power Co., and Japan Nuclear Cycle Development Institute. Kamioka Mining and Smelting Company provided services for activities in the mine.

[1] KamLAND Collaboration, A. Suzuki *et al.*, in *Proceedings of the 7th Euromicro Workshop on Parallel and Distributed Processing, Funchal, Portugal, 1999* [Nucl. Phys. (Proc. Suppl.) **B77**, 171 (1999)]; http://www.awa.tohoku.ac.jp/KamLAND/.

[2] Z. Maki *et al.*, Prog. Theor. Phys. **28**, 870 (1962).

[3] B. Pontecorvo, Sov. Phys. JETP **6**, 429 (1957) [Zh. Eksp. Teor. Fiz. **33**, 549 (1957)].

[4] J. N. Bahcall and R. Davis, Science **191**, 264 (1976); J. N. Bahcall, *Neutrino Astrophysics* (Cambridge University Press, Cambridge, United Kingdom, 1989); J. N. Bahcall, Astrophys. J. **467**, 475 (1996).

[5] F. Reines *et al.*, Phys. Rev. **117**, 159 (1960); for a review, see C. Bemporad *et al.*, Rev. Mod. Phys. **74**, 297 (2002).

[6] K. S. Hirata *et al.*, Phys. Rev. D **38**, 448 (1988).

[7] J. B. Benziger *et al.*, Nucl. Instrum. Methods Phys. Res., Sect. A **417**, 278 (1998).

[8] H. Kume *et al.*., Nucl. Instrum. Methods Phys. Res. **205**, 443 (1986).

[9] R. S. Raghavan *et al.*, Phys. Rev. Lett. **80**, 635 (1998).

[10] T. Hagner *et al.*., Astropart. Phys. **14**, 33 (2000).

[11] ^{235}U: K. Schreckenbach *et al.*, Phys. Lett. B **160**, 325 (1985); $^{239\,241}$Pu: A. A. Hahn *et al.*, Phys. Lett. B **218**, 365 (1989); ^{238}U: P. Vogel *et al.*, Phys. Rev. C **24**, 1543 (1981).

[12] B. Achkar *et al.*, Phys. Lett. B **374**, 243 (1996); G. Zacek *et al.*, Phys. Rev. D **34**, 2621 (1986).

[13] http://www.insc.anl.gov/

[14] P. Vogel and J. F. Beacom, Phys. Rev. D **60**, 053003 (1999); radiative correction from A. Kurylov *et al.*, hep-ph/0211306.

[15] Particle Data Group, Phys. Rev. D **66**, 010001-406 (2002).

[16] G. L. Fogli *et al.*., Phys. Rev. D **66**, 053010 (2002).

[17] M. Apollonio *et al.*, Phys. Lett. B **466**, 415 (1999).

[18] F. Boehm *et al.*, Phys. Rev. D **64**, 112001 (2001).

[19] L. Wolfenstein, Phys. Rev. D **17**, 2369 (1979); S. P. Mikheyev and A. Yu. Smirnov, Sov. J. Nucl. Phys. **42**, 913 (1986).

[20] A. de Gouvea *et al.*, Phys. Lett. B **490**, 125 (2000).